Published OnlineFirst July 15, 2020; DOI: 10.1158/1078-0432.CCR-20-1232

Evidencing a Pancreatic Ductal Adenocarcinoma Subpopulation Sensitive to the Proteasome Inhibitor Carfilzomib

Nicolas A. Fraunhoffer[1,2], Analía Meilerman Abuelafia[1], Martin Bigonnet[1], Odile Gayet[1], Julie Roques[1], Emmanuel Telle[1], Patricia Santofimia-Castaño[1], María Teresa Borrello[1], Eduardo Chuluyan[2,3], Nelson Dusetti[1], and Juan Iovanna[1]

ABSTRACT

Purpose: Pancreatic ductal adenocarcinoma (PDAC) is a lethal cancer with a survival rate less than 5%. Multiple chemotherapeutic drugs have been tested to improve patient prognosis; however, the clinical efficacy of these treatments is low. One of the most controversial family of drugs are the proteasome inhibitors, which have displayed promising effects in preclinical studies, but low clinical performance. Here, we unravel a specific transcriptomic signature that discriminates a subgroup of patients sensitive to the proteasome inhibitor carfilzomib.

Experimental Design: First, we identified a subpopulation of PDAC-derived primary cells cultures (PDPCC) sensitive to the proteasome inhibitor carfilzomib. Then, we selected a transcriptomic signature that predicts carfilzomib chemosensitivity using independent component analysis on the transcriptome of PDPCC. Finally, we validated the signature in an independent cohort of PDAC biopsy-derived pancreatic organoids.

Results: Sensitive phenotype was characterized by a high expression of genes related with a cornified/squamous pathway and a downregulation of epithelial–mesenchymal transition genes. Interestingly, carfilzomib-sensitive transcriptomic profile did not show any association with the proteasome activity but strongly correlates with ATF4 and CHOP expression, which are key markers of the unfolded protein response and critical to trigger the cell death program. Concordantly, sensitive phenotype showed a high level of the *de novo* RNA and protein synthesis compared with the resistant one and, most important, cell death induced by carfilzomib is dependent of the translational activity.

Conclusions: We demonstrate the existence of a carfilzomib-sensitive PDAC subgroup with a specific transcriptomic phenotype that could explain the biological reason for this responsiveness.

Introduction

Pancreatic ductal adenocarcinoma (PDAC) is the most frequent and lethal type of pancreatic cancer with a survival rate less than 5%, and it is projected to become the second cause of cancer-related death by 2030 (1, 2). This low survival is associated with late detection and presence of metastasis at diagnosis (3, 4). The main problem to face at the time of the diagnosis and treatment of this disease is the high heterogeneity among patients. Heterogeneity is related to a combination of malignant alterations at multiple levels of tumor biology, such as genetic, epigenetic, and microenvironmental factors (5–7). To address this issue, several studies have defined PDAC subtypes using transcriptomic and *multi-omics* data, allowing tumor stratification and identification of potential therapeutic targets (8–14). However, the application of this new knowledge to repurpose drugs in PDAC treatment is limited. In this context, we predicted and demonstrated the potential use of approved drugs, such as ezetimibe (15), bromodomain and extra-terminal inhibitors (BETi; refs. 13, 16), E2F inhibitors (12), and trifluoperazine (17). Following this rationale, the proteasome inhibitors (PI) are a promising group of drugs to assess for treating PDAC. PIs have shown high effect in preclinical studies both *in vitro* and *in vivo*, but poor clinical response in PDAC (18–22). Identifying a subgroup of PDAC sensitive to PIs and characterizing their molecular phenotype could help in increasing their clinical response through patient selection and by understanding the biological mechanism involved in the response.

The ubiquitin–proteasome system (UPS) is a critical factor in maintaining cell homeostasis through the degradation of unfolded or misfolded proteins, which ensure the cellular protein quality control, and is responsible for the removal of more than 80% of them (23, 24). A central component of the UPS is the proteasome 26S, which is composed by a 19S regulatory particle and a 20S core particle; the core particle contains three beta proteolytic subunits that mediate the protein degradation. A protein substrate for the UPS is marked with a polyubiquitin chain, which is recognized by the 19S proteasome subunit and then is translocated into the 20S proteolytic chamber for degradation (24–27). Disruption of UPS results in growth arrest and apoptosis-related to the activation of unfolded protein response (UPR).

[1]Centre de Recherche en Cancérologie de Marseille (CRCM), INSERM U1068, CNRS UMR 7258, Parc Scientifique et Technologique de Luminy, Aix-Marseille Université and Institut Paoli-Calmettes, Marseille, France. [2]Universidad de Buenos Aires, Consejo Nacional de investigaciones Científicas y Técnicas. Centro de Estudios Farmacológicos y Botánicos (CEFYBO). Facultad de Medicina. Buenos Aires, Argentina. [3]Universidad de Buenos Aires, Facultad de Medicina, Departamento de Microbiología, Parasitología e Inmunología, Buenos Aires, Argentina.

Note: Supplementary data for this article are available at Clinical Cancer Research Online (http://clincancerres.aacrjournals.org/).

N.A. Fraunhoffer and A.M. Abuelafia contributed equally to this article.

Corresponding Authors: Juan Iovanna, Centre de Recherche en Cancérologie de Marseille (CRCM), 163 Avenue de Luminy, Marseille 13288, France. Phone: 334-9182-8803; Fax: 334-9182-6083; E-mail: juan.iovanna@inserm.fr; and Nelson Dusetti, nelson.dusetti@inserm.fr

Clin Cancer Res 2020;26:5506–19

doi: 10.1158/1078-0432.CCR-20-1232

Published OnlineFirst July 15, 2020; DOI: 10.1158/1078-0432.CCR-20-1232

Translational Relevance

Pancreatic ductal adenocarcinoma (PDAC) low survival and minimal benefit of the current treatments have been associated with the high heterogeneity of this disease. Patient stratification and selection is a key factor to improve clinical outcomes. Proteasome inhibitors are a family of drugs with a high potential for PDAC treatment. However, their clinical results are variable. Transcriptomic data from PDAC-derived patient cell lines and organoids were used to generate and validate a signature that predicts the chemosensitivity to carfilzomib, a second-generation proteasome inhibitor. Interestingly, carfilzomib-sensitive phenotype is characterized for a squamous profile with a high capacity of unfolded protein response (UPR) induction, mediated for ATF4 and CHOP, and high translational levels. In contrast, the resistant phenotype expresses increased levels of epithelial–mesenchymal transition genes and a low UPR induction capacity. Altogether, these results provide a transcriptomic signature to use an FDA-approved drug for the treatment of patients with PDAC and potentially improve their clinical outcome. Furthermore, they validate the use of transcriptomics data from patient-derived models for the study of low frequency and lethal cancers.

Usually, cancer cells that have shown an elevated protein synthesis activity display a strong dependency on proteasome function because this process overloads the capacity of the endoplasmic reticulum to mediate protein folding (20, 24, 25, 28). Bortezomib, carfilzomib, and ixazomib PIs have been developed and approved for clinical use against multiple myeloma and mantle cell lymphoma. However, their efficacy in solid tumors is limited, probably due to their heterogeneity (20, 29).

Several studies have defined predictive markers of PIs sensitivity mainly in myeloma and breast cancer. These studies reported that the expression levels of antiapoptotic genes, such as MCL1 (30, 31) or the UPR capacity (32–35), are critical factors to determinate the PIs sensitivity. Despite the biological implications highlighted by these works, they do not show enough clinical efficiency.

In this work, we identified a specific transcriptomic signature that discriminates a subgroup of patients sensitive to carfilzomib using 20 PDAC-derived primary cell cultures (PDPCC), which was validated on 14 commercially available cell lines (CACL), and an independent cohort of biopsy-derived pancreatic organoids (BDPO). Moreover, the carfilzomib sensitivity was not correlated with the proteasome activity but showed an association with protein synthesis and UPR response.

Materials and Methods

PDAC samples and cell culture

The PDAC samples used in this work were obtained from three expert clinical centers after receiving ethics review board approval. Patients were included in this project under the PaCaOmics clinical trial (number 2011-A01439-32). Consent forms of informed patients were collected and registered in a central database. The studies were conducted in accordance with the Declaration of Helsinki.

Twenty PDPCCs were used in this study, thirteen as training cohort, and seven as validation cohort. These PDPCCs were obtained as described previously (15, 36). Patients' clinical data are detailed in Supplementary Tables S1 and S2. Briefly, PDAC samples were subcutaneously implanted in nude mice obtaining patient-derived xenografts (PDX). When PDXs reached 1 cm of diameter they were split into several small pieces (1 mm^3) and processed in a biosafety chamber. After a fine mincing, they were treated with collagenase type V (C9263; Sigma-Aldrich, Inc.) and trypsin/EDTA (25200-056; Gibco, Sigma-Aldrich, Inc.) and suspended in DMEM supplemented with 1% w/w penicillin/streptomycin (Gibco, Life Technologies) and 10% of FBS (Lonza). After centrifugation, cells were resuspended in serum-free ductal media (SFDM) adapted from Schreiber and colleagues (14) and conserved at 37°C in a 5% CO_2 incubator.

PDPCC sensitivity to proteasome inhibitors

Three thousand cells per well were seeded in 96-well plates in SFDM. Twenty-four hours later, the media were supplemented with increasing concentrations of BZT (Selleckchem), carfilzomib (Selleckchem), or ixazomib (Selleckchem) and incubated for 72 hours. Cell viability was measured with PrestoBlue (Thermo Fisher Scientific) reagent and quantified using the plate reader Tristar LB941 (Berthold Technologies). Each experiment was repeated at least three times. Eight increasing concentrations of PIs were used ranging from 0 to 5,950 nmol/L. Values were normalized and expressed as the percentage of the control (vehicle), which represents the 100% of normalized fluorescence.

Proteasome activity and proteasome inhibition assay

PDPCCs were cultured in SFDM and plated during 24 hours before starting the experiment at 10,000 cells per well in a 96-well plate. Proteasome activity was assessed by adding specific substrates (chymotrypsin-, trypsin-, and caspase-like), in the presence of luciferase using the Proteasome-Glo assay reagents according to the manufacturer's instructions. For the proteasome inhibition assay, PDPCCs were preincubated with PIs for 2 hours at 100 and 2,000 nmol/L. After, medium with PIs was removed and the proteasome activities were measured. Luminescence was detected using the plate read Tristar LB941 (Berthold Technologies), and values were normalized with the total cell viability measured by Presto Blue (Thermo Fisher Scientific).

PDPCC RNA extraction and RNA-seq analysis

PDPCC total RNA was extracted using RNeasy Mini Kit (Qiagen). RNA libraries were prepared (Illumina TruSeq RNA v2) and run on the Illumina High Seq-2000 for 101 bp paired end reads. Gene expression profiles were obtained using the MAP-RSeq v.1.2.1 workflow (37). MAP-RSeq consists of alignment with TopHat 2.0.626 against the human hg19 genome build and gene counts with the HTSeq software 0.5.3p9 (38) using gene annotation files obtained from Illumina. Gene counts were normalized using upper quartile. mRNA sequencing data are available under accession number EMBL-EBI: E-MTAB-5039.

Transcriptomic signature generation and differential gene expression analysis

Carfilzomib chemosensitivity signature was extracted using independent component analysis (ICA), which discriminates the biological relevant components from the transcriptome. ICA components were calculated on the PDPCC 10,000 most variant genes applying the JADE algorithm in MineICA R package (39). Pearson correlation was used to identify the component with the higher/significant association with carfilzomib chemosensitivity measured as base ten logarithm of

Published OnlineFirst July 15, 2020; DOI: 10.1158/1078-0432.CCR-20-1232

IC_{50}. The final signature was built with the genes that explain ≥3 SDs of the selected component distribution. To further confirm the gene profile associated with carfilzomib chemosensitivity, differential gene expression using EdgeR R package was performed on the PDPCC training cohort. Differential expressed genes (DEG) were extracted according to a $\log_2$ fold change ≥2 and an FDR < 0.05.

Functional analysis

To characterize the pathways related to the selected ICA component, a gene set enrichment analysis (GSEA) was performed using fgsea R package (40), which implements GSEA on a preranked list of genes and MsigDB signaling database (41). Pearson correlation was used to rank the genes according to the level of association among the ICA sample contribution matrix and the genes applied to extract the components. In addition, GSEA on DEGs was done through gene ontology (GO) analysis and pathway analysis on Reactome databases using the R packages, ClusterProfiler and ReactomePA, respectively.

Cell line microarray and chemosensitivity data analysis

CEL microarray files for 21 pancreatic cancer CACL were downloaded from ArrayExpress database (E-MTAB-3610). Microarray data were processed following the workflow detailed in the maEndToEnd R package. Briefly, oligo R package was used to read and perform background subtraction and normalization of probe set intensity applied by the Robust Multi-array Analysis (RMA). Then, common cell lines with the Dependency Map chemosensitivity database (DepMap) were used ($n = 14$) for carfilzomib chemosensitivity signature validation. For each cell line, effective concentration 50 (EC_{50}) was extracted from PRISM Repurposing Secondary Screen 19Q4 database.

Transcriptomic subtype classification and carfilzomib signature association

The Moffitt–Purist classification was applied to normalized data using the published weights for each gene (13). A centroid classifier approach was used for Chan-Seng-Yue (14), Collisson (9), and Bailey (8) subtype classification. Centroid was calculated using K-means on ICGC RNA-seq database (PACA-AU), previous sample selection according to the expression profile of each subtype measured by hierarchical clustering on principal components from FactoMineR R package. After that, the subtypes were predicted for the new datasets using the "cl_predict" function from clue R package. To measure the association with a specific transcriptomic subtype, Pearson correlation coefficients were calculated among the normalized counts of the genes used for the classification and the contribution of each sample to the signature in the training cohort.

De novo in-cell RNA and protein synthesis

Initially, 5,000 cells/well were seeded in 8-well μ-slides (BD Biosciences) and incubated for 24 hours before treatment. Then, the cells were treated with the vehicle or carfilzomib 100 nmol/L for 3 and 6 hours. To determine the nascent ARN and protein, CuAA Cell Reaction Buffer Kit was used (Jena Bioscience). Nascent protein and RNA were marked for its detection with an alkyne containing ethynyl-labeled uridine or O-propargyl-puromycin (OP) probe, respectively. Detection is based on a click reaction with a fluorescent azide. The reaction was conducted according to the manufacturer's instructions. Reaction visualization and image acquisition were done at 20× and 40× with a Nikon eclipse 90i microscope (Nikon), and the fluorescent intensity was quantified by NIH Image J software (42).

De novo protein synthesis inhibition

To evaluate the impact of PDPCC's protein translation on the chemosensitivity against carfilzomib, 3,000 cells/well were plated in a 96-well plate 24 hours before the start of the experiment. The protein synthesis was inhibited with 4 μg/mL of puromycin for 2 hours. After that, the cells were cultured with vehicle and carfilzomib at two concentrations, 2,000 and 5,000 nmol/L for 24 hours. Cell viability was measured with PrestoBlue (Thermo Fisher Scientific) reagent quantified using the plate reader Tristar LB941 (Berthold Technologies). Values were normalized and expressed as the percentage of the control.

Protein extraction and Western blot analysis

To perform protein expression analysis, the cells were treated during 3 and 6 hours with vehicle or 100 nmol/L of carfilzomib. Then, the cells were detached and homogenized in RIPA buffer. The proteins were separated by SDS-PAGE (29:1 acrylamide:bis-acrylamide, Euromedex Laboratories) in 10% to 12% running gel and 4% stacking gel, in an electrophoresis cell. Proteins were electrotransferred to a nitrocellulose membrane (Immobilon-P, EMD Millipore Corporation) at 250 mA for 2 hours. To identify proteins, the membranes were blocked for 1 hour at room temperature with 5% powdered milk in PBS containing 0.1% Tween 20. Next, they were incubated overnight at 4°C with the rabbit polyclonal antibodies anti-ATF4 (1:1,000; Cell Signaling Technology), anti-ATF6 (1:2,000; Cell Signaling Technology), and the goat polyclonal antibody anti-CHOP (1:1,000; Cell Signaling Technology). For the immunoreaction, the membranes were incubated with horseradish peroxidase (HRP)-conjugated goat anti-rabbit IgG (1:3,000 dilution, Suther Biotech) or HRP-conjugated rabbit anti-goat IgG (1:3,000 dilution, Suther Biotech). The outcome was visualized using the Chemiluminescent HRP substrates (Millipore Corporation) for chemiluminescence development. To normalize the results, monoclonal anti-β-tubulin (1:6,000 dilution, Sigma-Aldrich, Inc.) was used on the same membranes and revealed with HRP-conjugated goat anti-mouse IgG (1:3,000 dilution, Suther Biotech). The membranes were scanned using a PXi multi-application imager (Sygene). The estimation of bands was performed using a prestained protein ladder (SeeBlue Plus2, Thermo Fisher Scientific) as a molecular weight marker. The intensity of each protein band was quantitated using the NIH Image J software (42), and the results were expressed as the optical density of each protein/optical density of β-tubulin.

Immunofluorescence and nuclear localization quantification

Five thousand cells/well were seeded in 8-well μ-slides (BD Biosciences) and incubated 24 hours before treatment. The cells were treated with the vehicle or carfilzomib at a concentration of 100 nmol/L for 3 and 6 hours. After that, the medium was removed, and the cells were fixed with cold methanol for 15 minutes at 4°C. Previous to the incubation with the primary antibodies, cells were washed twice with PBS and with blocking serum solution (Vector Laboratories) diluted in 1.5% PBST for 30 minutes. Then, the cells were incubated with the primary antibody overnight at 4°C. The primary antibodies used were rabbit polyclonal anti-ATF4 (1:100 Cell Signaling Biotechnology), anti-ATF6 (1:200 Cell Signaling Biotechnology), and goat anti-CHOP (1:100; Cell Signaling Biotechnology). The secondary antibodies used were Alexa 488–conjugated anti-rabbit (1:400; Invitrogen, Thermo Fisher Scientific) and Alexa 488–conjugated anti-goat (1:400; Thermo Fisher Scientific), which were incubated with the sections for 60 minutes at room temperature. The slides were counterstained with mounting medium for fluorescence with DAPI (H-1,200; Vector Laboratories). Negative controls were processed in the same manner with omission of the primary antibodies. One hundred cells were

Published OnlineFirst July 15, 2020; DOI: 10.1158/1078-0432.CCR-20-1232

selected randomly to quantify the nuclear signal of ATF6, ATF4, and CHOP. Images were captured using an optical microscope (Eclipse 90i; Nikon) with an attached digital camera (DXM1200C; Nikon).

UPR genes signature analysis

The gene sets for UPR (M5922), ATF6 (M27284), PERK (M2781), ATF4 (M796), and CHOP (M1477) were extracted from MsigDB signaling database (41). The normalized, gene-wise zero-centering, and unit variance scaling gene counts were plotted according to the resistant and sensitive phenotype in the training cohort. In addition, Pearson correlation coefficients were calculated among the normalized counts of the genes that compose the ATF6, PERK, ATF4, and CHOP gene sets and the contribution of each sample to the signature.

Biopsy-derived pancreatic organoid generation, RNA extraction, and RNA-seq analysis

BDPOs were obtained from 22 consecutive endoscopic ultrasound-guided fine-needle aspirations (EUS-FNA) from patients with PDAC. Briefly, PDAC cells were obtained from the biopsies through slight digestion with the Tumor Dissociation Kit (Miltenyi Biotec) at 37°C for 5 minutes. Isolated cells were placed into 12-well plates coated with 150 μL growth factor–reduced Matrigel (Corning) and cultured with advanced DMEM/F12 supplemented with HEPES (10 mmol/L; Thermo Fisher Scientific), human recombinant FGF10 (100 ng/m; PeproTech), human recombinant EGF (50 ng/mL; PeproTech), human recombinant Noggin (100 ng/mL; Bio-Techne), human Gastrin 1 (10 nmol/L; Sigma-Aldrich, Inc.), Nicotinamide (10 mmol/L; Sigma-Aldrich, Inc.), N-acetylcysteine (1.25 mmol/L; Sigma-Aldrich, Inc.), B27 (Thermo Fisher Scientific), A83-01 (500 nmol/L; Bio-Techne), and Y27632 (10.5 μmol/L; Bio-Techne). The plates were incubated at 37°C in a 5% CO_2 incubator, and the media changed every 3 to 4 days. Total RNA was extracted using RNeasy Mini Kit and RNA libraries were prepared as described above. Gene expression profiles were obtained using the MAP-RSeq v.1.2.1 workflow as described above. Gene counts were normalized using upper quartile.

Signature projection

The signature projection on PDPCC, CACL, and BDPO transcriptome was performed using the MASS R package (43). A score that classifies PDPCC, CACL, and BDPO according to the degree of chemosensitivity was calculated applying the cross-product among the Moore–Penrose generalized inverse of the gene contribution to the signature and the RNA expression matrix.

BDPO carfilzomib chemosensitivity

BDPOs were disaggregated with accutase (Thermo Fisher Scientific), and 1,000 cells/well were plated in a 96-well round bottom ultra-low plate (Corning) with the medium described above. Twenty-four hours later, the media was supplemented with increasing concentrations of carfilzomib (Selleckchem) and incubated for 72 hours. Cell viability was measured with CellTiter-Glo 3D (Promega) reagent quantified using the plate reader Tristar LB941 (Berthold Technologies). Each experiment was repeated at least three times. Eight increasing concentrations of PIs were used ranging from 0 to 5,950 nmol/L. Values were normalized and expressed as the percentage of the control (vehicle), which represent 100% of normalized fluorescence.

Time-lapse analysis

To validate the carfilzomib chemosensitivity on BDPOs, we performed 72-hour time-lapse video microscopy on one carfilzomib-sensitive (PDAC104T) and one resistant BDPO (PDAC109T) with 10 and 2,000 nmol/L of carfilzomib. Cell viability was measured using two dyes: IncuCyte NucLight Rapid Red for living cells (Sartorius) and IncuCyte Cytotox green reagent for death cells (Sartorius). Celldiscoverer 7 microscope (Zeiss) was used for image acquisition and the fluorescent intensity was quantified by NIH Image J software (42). Fluorescent values were normalized and expressed as the percentage of the control.

Statistical analysis

The inhibitory concentration 50 (IC_{50}) values, AUC, logarithm base 10 transformation for IC_{50}, EC_{50}, and Bartlett test for sphericity were performed in Prism 8.3 (GraphPad). Pearson correlation coefficients and the significance levels were calculated using the Hmist R package. Mann–Whitney test and Kruskal–Wallis test were performed with R basic functions. Correlograms and the heatmaps were built with ggplot2 and ComplexHeatmap R packages (44, 45), respectively.

Results

Characterization of PDPCC PIs sensitivity

An *in vitro* cytotoxic assay was performed in 13 PDPCCs with 3 different PIs (carfilzomib, bortezomib, and ixazomib) to analyze their differential sensitivity. The clinical characteristics of patients from where PDPCCs were derived are displayed in Supplementary Table S1. PDPCCs showed a different pattern of sensitivity to PIs (**Fig. 1A**) measured by IC_{50} and AUC (Supplementary Table S1). However, Pearson correlation coefficient was significantly high for bortezomib and ixazomib for both $\log IC_{50}$ ($r = 0.66$; $P = 0.01$; **Fig. 1B**) and $\log_{AUC}$ ($r = 0.62$; $P = 0.01$; **Fig. 1B**), whereas carfilzomib did not correlate with the other PIs.

To stratify PDPCCs with respect to PI sensitivity, we analyzed whether the $\log IC_{50}$ or the log-AUC captures the variability observed in the chemograms. Variability evaluated by Bartlett test showed that $\log IC_{50}$ was the parameter that better characterized the variability among PIs ($P < 0.0001$; **Fig. 1C**). Thus, we used $\log IC_{50}$ to stratify the PDPCC according to PI sensitivity. Stratification was performed by grouping the $\log IC_{50}$ for the three PIs establishing one SD as a threshold to determine the most and less responsive groups. Carfilzomib was the only drug that showed a discriminative pattern of sensitivity among PDPCCs with 23% ($n = 3$) and 77% ($n = 10$) classified as sensitive and resistant, respectively (Supplementary Table S1; **Fig. 1C**).

Deriving a transcriptomic signature to predict carfilzomib sensitivity

A specific transcriptomic phenotype associated to carfilzomib sensitivity was detected using ICA decomposition on a set of 12 transcriptomes derived from the previous chemosensitivity evaluation (**Fig. 1C**). The ICA algorithm was applied on the 10,000 most variant genes and the presence of five components (ICA1-ICA5) was revealed. ICA1 and ICA3 showed a strong association with patients' age (**Fig. 2A**). ICA4 was the only component that correlated significantly with carfilzomib $\log IC_{50}$ ($r = 0.69$; $P = 0.013$; **Fig. 2A**). Ninety-five genes that explain ≥3 SDs of ICA4 were selected to constitute carfilzomib chemosensitivity signature (Supplementary Table S2). Applying unsupervised K-means clustering on the signature revealed two PDPCC subgroups with a specific gene profile (**Fig. 2B**). Carfilzomib-sensitive PDPCCs were enriched in keratins (KRT), kallikreins (KLK), and small proline-rich proteins (SPRR), whereas the resistant subgroup showed a higher expression of VIM, CDH2, and POSTN

Published OnlineFirst July 15, 2020; DOI: 10.1158/1078-0432.CCR-20-1232

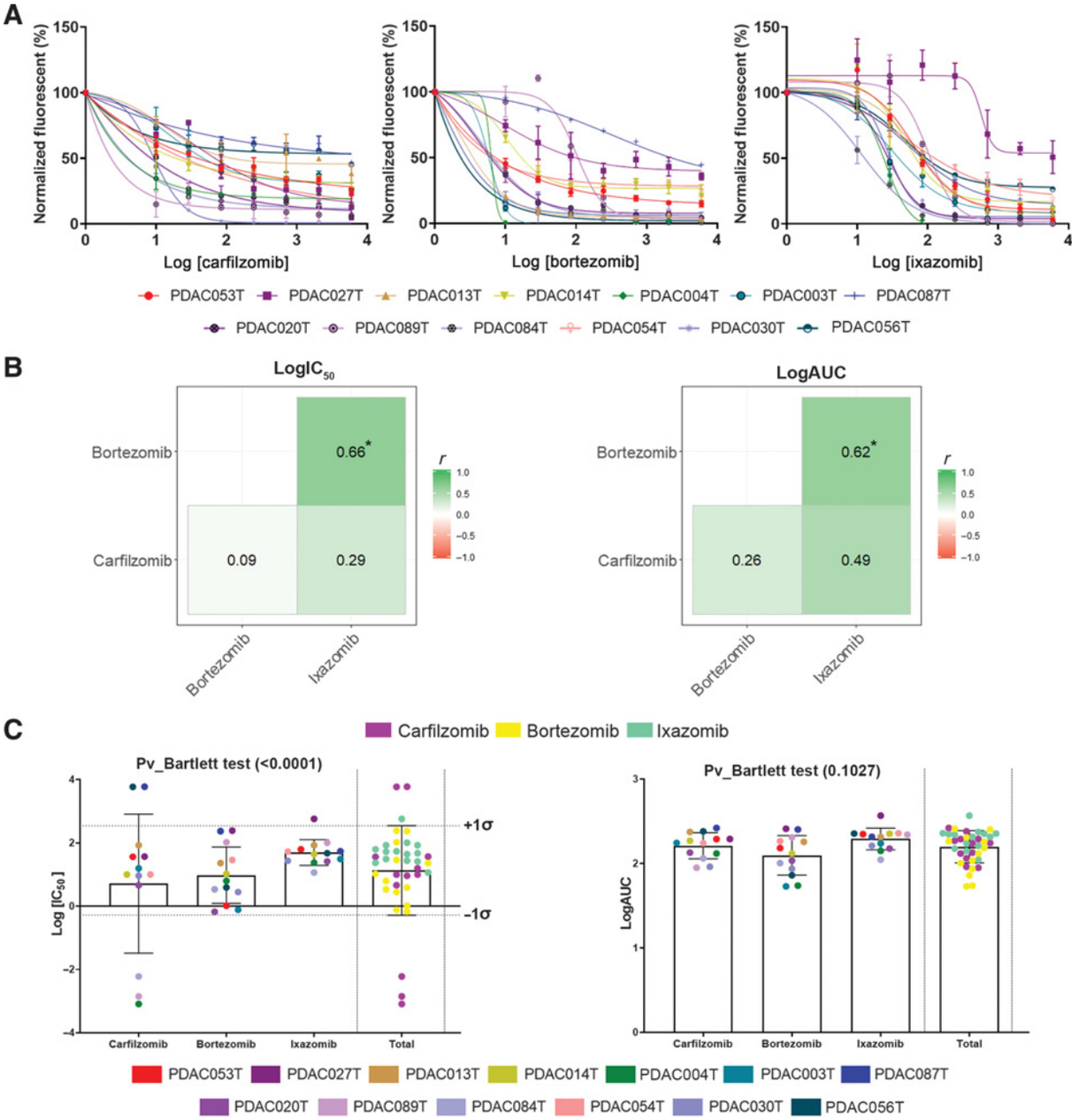

Figure 1.

Characterization of chemosensitivity profile after proteasome inhibitors treatment in PDPCC. **A,** Chemosensitivity analysis of the proteasome inhibitors carfilzomib, bortezomib, and ixazomib on 13 PDPCC. **B,** Correlation between bortezomib and ixazomib measured with Pearson correlation showed a high correlation among bortezomib and ixazomib, both $logIC_{50}$ ($r = 0.66$; $P = 0.01$) and logAUC ($r = 0.62$; $P = 0.01$), while carfilzomib did not correlate with the other inhibitors. **C,** $LogIC_{50}$ is the chemosensitivity parameter that characterizes the variability among the proteasome inhibitors using Bartlett test ($P < 0.0001$). Chemograms and boxplots from **A** and **C**, respectively, are plotted as the mean ± SD. *, $P < 0.05$.

(**Fig. 2B**; Supplementary Table S2). Pathway analysis showed that the sensitive PDPCCs have increased levels of genes related with a cornified/squamous phenotype (NES = 2.63; FDR = 0.01; **Fig. 2C**), associated with a downregulation of epithelial–mesenchymal transition (EMT) genes (NES = −2.09; FDR = 0.03; **Fig. 2C**). These observations were confirmed through differential expression analysis with the detection of 358 DEGs, which were related with cornification (GO:0001533; FDR = 0.02) and keratinization pathways (R-HSA-6805567; FDR < 0.0001), detected by GO and Reactome pathway analysis, respectively (Supplementary Fig. S1; Supplementary Table S3). Although the signature is enriched in genes/pathways related to a basal/squamous subtype, it was not detected in a statistical association with this phenotype or another across the different transcriptomic classifications (Supplementary Fig. S1F).

Published OnlineFirst July 15, 2020; DOI: 10.1158/1078-0432.CCR-20-1232

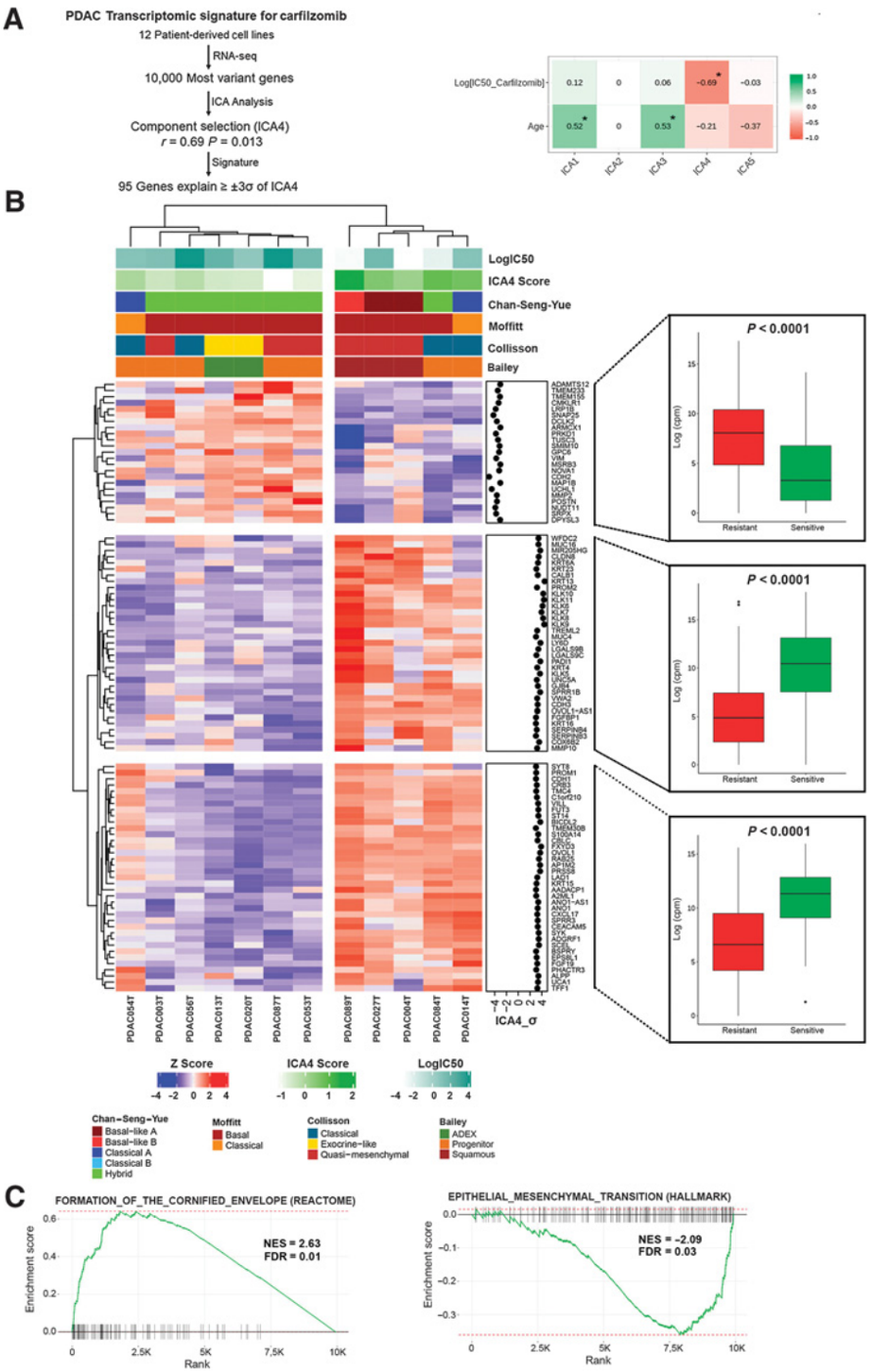

Figure 2.

Carfilzomib chemosensitivity signature identification. **A,** ICA on 12 PDPCC RNA-seq. ICA4 is the component with the highest correlation with carfilzomib logIC$_{50}$ ($r = 0.69$; $P = 0.013$). **B,** Ninety-five genes explained more than 3 times the variability to carfilzomib sensitivity among PDPCC and displayed a clear phenotypic discrimination among the resistant and sensitive subgroups. Boxplots describe the difference in total gene expression measured as the logarithm base 2 of counts per million among resistant and sensitive PDPCC. **C,** GSEA analysis revealed that the sensitive PDPCC are enriched in genes associated with a cornified/squamous phenotype (NES = 2.63; FDR = 0.01) and a reduction in epithelial–mesenchymal transition genes (NES = −2.09; FDR = 0.03). Boxplots are plotted as the median and the extremes represent the first and third quartile, respectively. *, $P < 0.05$ (Mann–Whitney test).

Carfilzomib chemosensitivity signature was validated in 7 additional PDPCCs, and an external cohort of 14 CACL in which transcriptomes (Supplementary Table S1; Supplementary Table S2) were projected on ICA4 component to calculate a chemosensitivity score (Supplementary Fig. S2). Both PDCC and CACL projected scores highly correlate with the logIC$_{50}$ ($r = -0.84$; $P = 0.01$; Supplementary Fig. S2A) and logEC$_{50}$ ($r = -0.76$; $P = 0.002$; Supplementary Fig. S2B), respectively. Altogether, these results confirm the presence of a PDAC subgroup sensitive to carfilzomib, which is not related to a specific subtype.

Proteasome activity and chemosensitivity to PIs in PDPCCs

The reduction of proteasome activity and PI resistance have been associated with a pro-mesenchymal phenotype (27, 46).

Published OnlineFirst July 15, 2020; DOI: 10.1158/1078-0432.CCR-20-1232

Interestingly, the carfilzomib sensitivity PDPCC subgroup showed a strong downregulation of EMT genes. Thus, to evaluate the association between proteasome activity and carfilzomib chemosensitivity, we measured chymotrypsin-, trypsin-, and caspase-like activity in PDPCCs (**Fig. 3A**). Chymotrypsin-like was the main activity detected (61.07% ± 10.17%), whereas trypsin-like was the lowest (12.77% ± 4.40%). Next, we analyzed the association among PIs' sensitivity and the proteasome activities using Pearson correlation. Only bortezomib correlated marginally with the proteasome activities (**Fig. 3A**), indicating that the proteasome activity is not a critical modulator of carfilzomib sensitivity. To further analyze the differential impact of carfilzomib on proteasome

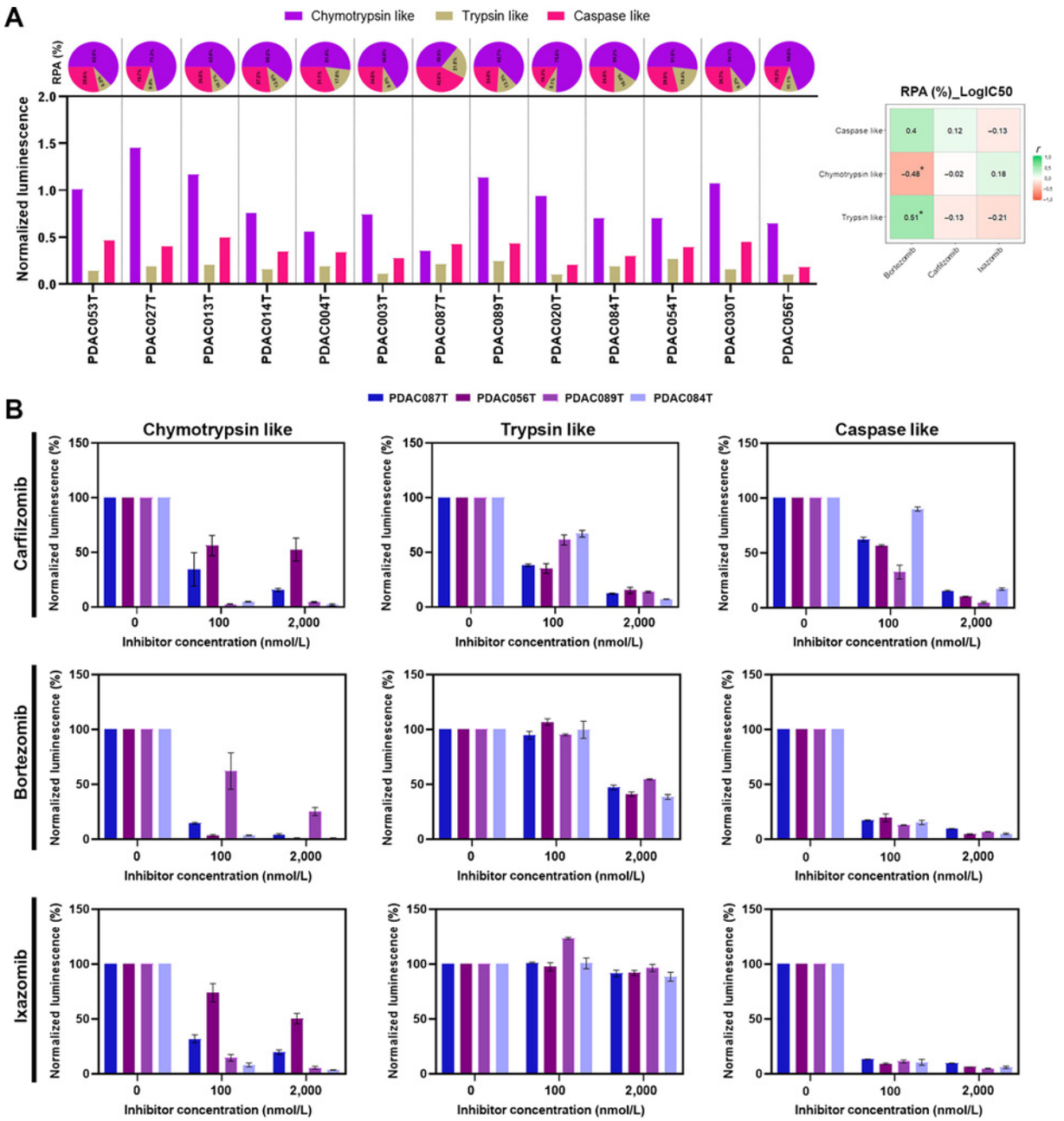

Figure 3.

Proteasome activity before and after treatment of PDPCC. **A,** Proteasome activities were measured in the training PDPCC group and correlated with the $logIC_{50}$ of bortezomib, carfilzomib, and ixazomib. **B,** Proteasome activity inhibition was evaluated in four PDPCC, two resistant (PDAC087T and PDAC056T) and two sensitive (PDAC089T, and PDAC084T) at two concentrations (100 and 2,000 nmol/L) for carfilzomib, bortezomib, and ixazomib. Bar plots in **A** represent the proteasome normalized by cell viability and the pie plots show the relative proteasome activity (RPA) as proportion of the total measured activity. Bar plots in **B** are represented as percentage in relation to the control (vehicle). *, $P < 0.05$.

Published OnlineFirst July 15, 2020; DOI: 10.1158/1078-0432.CCR-20-1232

activity related to the chemosensitivity phenotypes, two carfilzomib-sensitive (PDAC089T and PDAC084T) and two carfilzomib-resistant (PDAC087T and PDAC056T) PDPCCs were treated with the three PIs at two concentrations, 100 and 2,000 nmol/L, for 2 hours, and after that, proteasome activities were measured (**Fig. 3B**). As we expected, all PIs showed a potent inhibition of chymotrypsin-like activity even at 100 nmol/L with the highest effect on the sensitive PDPCCs. The caspase-like activity was negatively modulated by the three PIs independently of the phenotype, whereas trypsin-like was affected for carfilzomib at 100 nmol/L only. These results suggest that the pan-inhibition of the carfilzomib on the three proteasome activities could explain the presence of a specific PDPCC subgroup with a high sensitivity to this PI.

UPR activity response correlates with carfilzomib chemosensitivity phenotype

Previous studies have shown induction of UPR as a mechanism of chemosensitivity to PI treatment in pancreatic cancer cell lines (17, 35, 47, 48). We expanded these studies examining UPR response in two resistant (PDAC056T and PDAC087T) and two sensitive (PDAC084T and PDAC089T) PDPCCs with two carfilzomib concentrations (50 and 100 nmol/L) at 3 and 6 hours. The resistant PDPCCs showed a low capacity of UPR response (**Fig. 4**; Supplementary Fig. S3). Carfilzomib-resistant phenotype was related with high levels of the endoplasmic reticulum (ER) chaperone GRP78 and a reduced induction of UPR-related transcriptional factors ATF6, ATF4, and CHOP in the presence of carfilzomib (**Fig. 4A** and **B**; Supplementary Fig. S3A). Following the rationale, we quantify the nuclear localization of the study UPR-related transcriptional factors at 100 nmol/L of carfilzomib at 3 and 6 hours (**Fig. 4C**). Despite this, ATF6 protein expression increased in the sensitive PDPCCs at 6 hours; the nuclear ATF6 was higher in the resistant PDPCCs with 75% ± 2% of positive nuclei, whereas the sensitive PDPCCs showed a peak at 3 hours with a cytoplasmatic accumulation of ATF6 at 6 hours. Contrarily, nuclear localization for ATF4 was lower in the resistant PDPCC than the sensitive one at 6 hours. CHOP followed ATF4 pattern with 83% ± 1% of positive nuclei in the sensitive PDPCCs. To further understand the mechanism associated with the differential UPR response among carfilzomib-resistant and -sensitive subgroups, the expression levels of the gene sets of UPR, ATF6, PERK/ATF4, and CHOP extracted from MsigDB signaling database were analyzed. Globally, the UPR gene set did not show statistical differences among subgroups ($P = 0.420$; Supplementary Fig. S3B). However, genes related to ATF6 (Supplementary Fig. S3C), PERK/ATF4 (Supplementary Fig. S3D), and CHOP (Supplementary Fig. S3E) showed statistical differences. Specifically, high levels of chaperones (HSP90B1 and HSP5/GRP78) were observed in the resistant subgroup. In contrast, the expression of genes related to RNA processing (EXOSC proteins) and translational regulation (PPP1R15A/GADD34) was increased in the sensitive subgroup. Pearson correlation confirmed these observations among the expression of UPR-related genes and the carfilzomib ICA4 score (Supplementary Table S3). These results suggest that the carfilzomib chemosensitivity phenotype revealed by the ICA analysis is related to a differential UPR response pattern and ER stress–induced apoptosis in PDPCCs.

De novo RNA and protein synthesis in PDPCC

Protein synthesis levels play a critical role in PI sensitivity and UPR induction (48, 49); due to this fact, we examined the levels of *de novo* RNA and protein synthesis basally and after 100 nmol/L carfilzomib treatment at 3 and 6 hours. The levels of RNA and protein synthesis were higher in the sensitive PDPCCs than resistant PDPCCs with an increase of 54% ($P = 0.002$) and 89% ($P < 0.0001$), respectively (**Fig. 5A** and **B**). Interestingly, carfilzomib treatment did not significantly modify the RNA or protein synthesis at either 3 or 6 hours (**Fig. 5A** and **B**). To further confirm the effect of protein synthesis on carfilzomib chemosensitivity, we inhibited protein translation with 4 μg/mL of puromycin and measured cell viability after carfilzomib treatment at 2,000 and 5,000 nmol/L. Sensitive PDPCCs treated with puromycin showed a significant increase in the cell viability both at 2,000 and 5,000 nmol/L (**Fig. 5C**).

Validation of carfilzomib chemosensitivity in BDPOs

Twenty PDAC patient BDPOs were used to confirm the carfilzomib chemosensitivity signature extracted from the PDPCCs. Initially, the BDPO transcriptomes were projected on the carfilzomib signature applying the ICA4 component (Supplementary Table S2). Then, six BDPOs were selected to test their carfilzomib sensitivity. Clinical data are available in Supplementary Table S1. A high correlation was observed between the carfilzomib sensitivity pattern and the projected ICA4 score ($r = -0.92$; $P = 0.01$; **Fig. 6**). The three BDPOs classified as sensitive showed a lower IC_{50} and AUC than the BDPOs scored as resistant (**Fig. 6A** and **B**). In addition, cell viability was measured in a 72-hour time-lapse video microscopy. As expected, a strong response to carfilzomib was observed in the BDPOs scored as sensitive (PDAC104T) with an almost complete reduction of the cell viability at 48 hours posttreatment even at 10 nmol/L (**Fig. 6C**; Supplementary Video S1). Contrarily, the organoid scored as resistant (PDAC109T) showed a cell viability near to 100% at the end of the experiment (**Fig. 6D**; Supplementary Video S2). All these results confirmed the reliability of the signature to predict the PDAC sensitivity to carfilzomib.

Discussion

Despite being an overall dismal cancer, the clinical outcome of pancreatic adenocarcinoma is difficult to anticipate principally due to the huge heterogeneity that this tumor presents. An accurate predictive method applicable for all patients would greatly improve individual care by identifying the most appropriate course of treatment. In fact, RNA has an unrecognized and extensive potential for personalized clinical management of patients with cancer. Indeed, the molecular classification of pancreatic adenocarcinoma is still a highly debated subject, with broad discordances between subtyping systems. High-throughput data have contributed to generate a novel classification and identify new cellular and molecular biomarkers in PDAC (6, 8–15). However, specific chemosensitivity signatures that predict the response to clinically approved drugs are poorly characterized. Several studies have proved a strong correlation among PDAC transcriptional profile, drug response, and clinical survival (15, 36, 50). In this work, we identify a subgroup of PDAC sensitive to carfilzomib and unravel a transcriptomic predictive signature identifying them.

PDAC sensitivity to bortezomib has been characterized extensively, even at a clinical level, with poor and uncertain results, which have been related with low drug penetration, mutations, or overexpression of β5 subunit and the presence of multidrug efflux transporters (18, 19, 23, 25, 29, 50, 51). This lack of clear results has set aside the other PIs as PDAC therapeutic drugs. Using a panel of 13 PDPCCs, we characterized an *in vitro* chemosensitivity profile for the three FDA-approved PIs. The general sensitivity among the

Published OnlineFirst July 15, 2020; DOI: 10.1158/1078-0432.CCR-20-1232

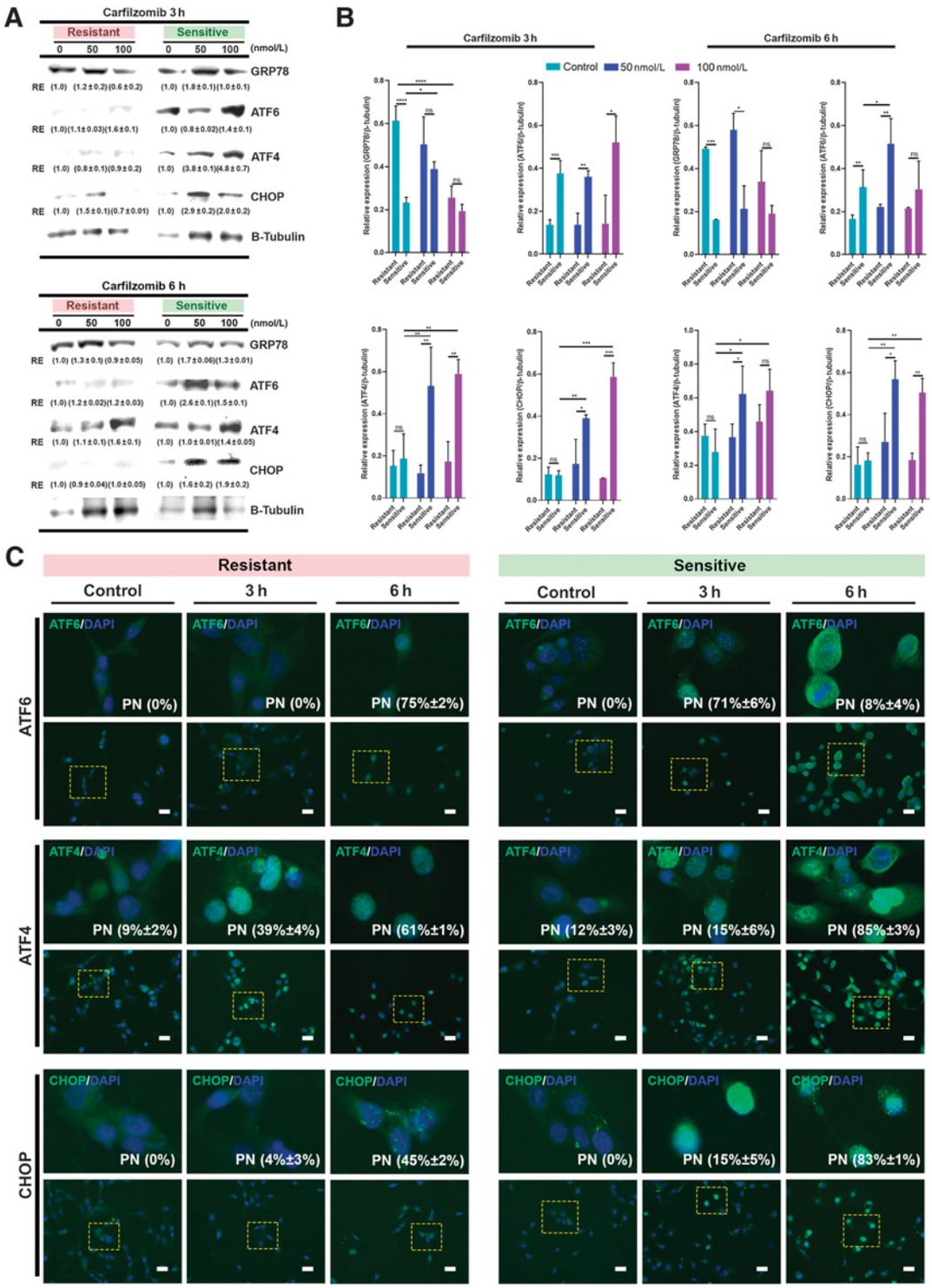

Figure 4.

UPR correlates with carfilzomib chemosensitivity signature. **A,** Western blot analysis of GRP78, ATF6, ATF4, and CHOP comparing their expression among a resistant (PDAC056T) and sensitive (PDAC084T) PDPCC after carfilzomib treatment (50 and 100 nmol/L) at two time points, 3 and 6 hours. **B,** Western blot quantification comparing PDPCC resistant and sensitive subgroups. **C,** Immunofluorescence of ATF6, ATF4, and CHOP and quantification of nuclear signal comparing resistant and sensitive PDPCC. Scale bar, 50 μm. Bar plots in **B** are plotted as the mean ± SD. ns, no significance; RE, relative expression. *, $P < 0.05$; **, $P < 0.01$; ***, $P < 0.001$; ****, $P < 0.0001$ (Mann–Whitney test).

Published OnlineFirst July 15, 2020; DOI: 10.1158/1078-0432.CCR-20-1232

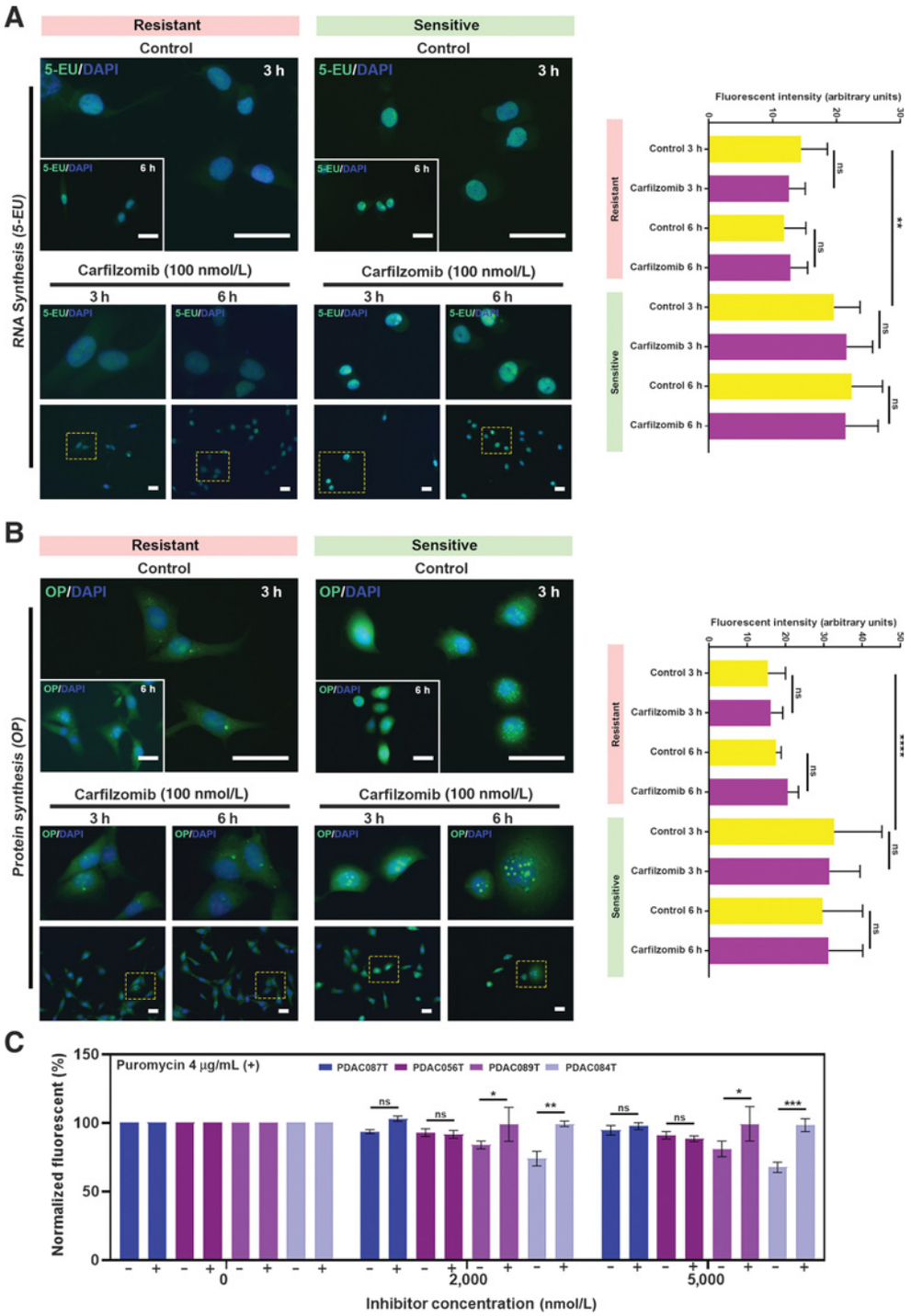

Figure 5.

De novo RNA and protein synthesis in relation to carfilzomib chemosensitivity phenotype. **A** and **B** show the RNA and protein synthesis measured for a click reaction with a fluorescent azide. **C,** Inhibition of protein synthesis with puromycin rescue the sensitive PDPCC after 24 hours of treatment with 2,000 and 5,000 nmol/L of carfilzomib. Scale bar, 50 μm. Bar plots in **A** and **B** are plotted as the mean ± SD. 5-EU, ethynyl-labeled uridine; ns, no significance; OP, O-propargyl-puromycin. *, $P < 0.05$; **, $P < 0.01$; ***, $P < 0.001$; ****, $P < 0.0001$ (Mann–Whitney test).

Published OnlineFirst July 15, 2020; DOI: 10.1158/1078-0432.CCR-20-1232

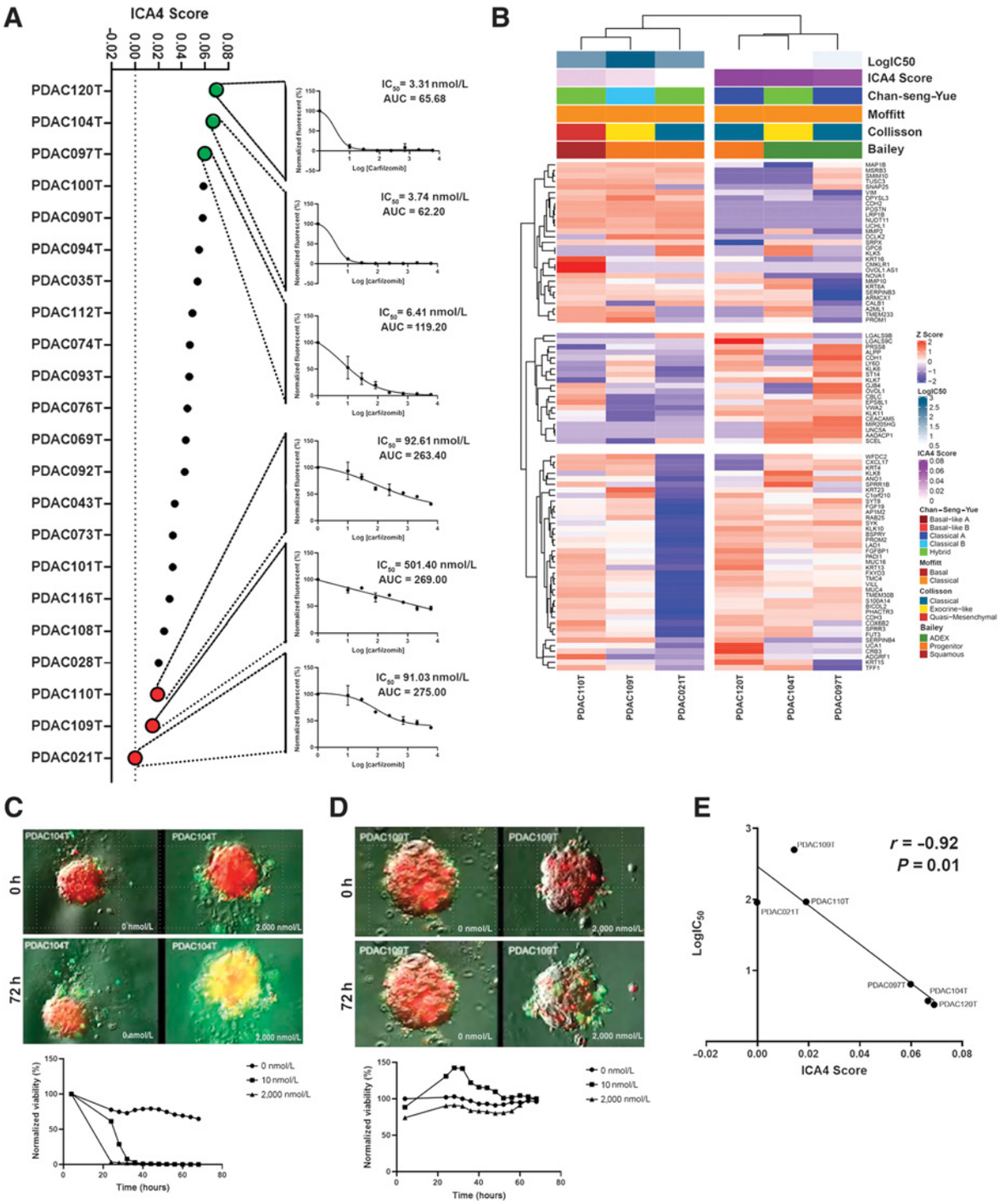

Figure 6.

Validation of carfilzomib chemosensitivity signature using BDPO. **A** and **B,** BDPO transcriptomes were projected on ICA4 to calculate a chemosensitivity score which were validated with an *in vitro* chemosensitivity assay. **C** and **D,** BDPO chemosensitivity profile was confirmed by a time-lapse experiment with a sensitive (PDAC104T) and resistant (PDAC109T) BDPO for 72 hours at two concentrations (10 and 2,000 nmol/L). **E,** BDPO $logIC_{50}$ correlates significantly with the projected ICA4 score ($r = -0.92$; $P = 0.01$). Scatter plot are plotted as the mean ± SD and normalized in relation to the control (vehicle).

three inhibitors was markedly different across the PDPCCs. Carfilzomib and bortezomib showed the lowest IC_{50}, whereas ixazomib's cytotoxic activity was observed at higher concentrations. However, the variability in the sensitivity was lower with bortezomib and ixazomib than carfilzomib. As we expected, most of PDPCCs fell as intermediate responders for all the PIs, while carfilzomib was the only PI defining a significantly sensitive PDAC subgroup.

Transcriptomic analysis using the ICA algorithm demonstrated the existence of a gene signature that discriminates carfilzomib-sensitive and -resistant subgroups without being associated with a specific transcriptomic subtype. This chemosensitivity-predictive signature is composed of 95 genes that correlate with the PDPCC EMT status. Sensitive cells are enriched in epithelial-associated genes such as KRTs, KLKs, and SPRRs, whereas resistant PDPCCs showed a pro-mesenchymal profile. These observations are consistent with previous studies that have observed that the PI resistance is associated with the EMT induction capacity and the differentiation state (46). However, our results contrast with Genovese and colleagues, who, using a SMARCB1 deficient subpopulation of mice pancreatic cancer–derived cells, observed an association among an increase in mesenchymal markers and a high sensitivity to PI (52). These might be explained due to the fact that Genovese and colleagues performed their analysis in a particular subpopulation of tumoral cells derived from senescence escaper clones, which do not recapitulate the real phenotypic heterogeneity of human pancreatic cancer, in which multiple cell populations with different phenotypes and EMT status could coexist (14), whereas the carfilzomib chemosensitivity signature was identified and validated using the global transcriptomic heterogeneity gradient without pointing out a specific cell subpopulation. Thus, the carfilzomib-sensitive phenotype could be related to a differentiation degree, which is not transcriptomic subtype dependent and has low EMT induction capacity. In contrast with other types of solid tumors that have displayed a strong correlation among PI sensitivity and proteasome activity (20, 24, 52), PDPCC sensitivity to carfilzomib did not correlate with proteasome activity. However, carfilzomib was the only PI that targeted the trypsin-like activity, a factor that has been postulated as central for the use of PIs in solid tumors (53, 54).

PIs affect the cancer cells in multiple ways, such as NF-κB inactivation and cell-cycle arrest (20, 25, 26, 29). However, UPR is crucial to trigger the cellular events that culminate with the activation of the cell death program. PIs promote severe ER stress, associated with ATF4 expression, which leads to the transcription of CHOP, a transcriptional factor that induces proapoptotic protein (48, 49). Here, we demonstrated that the carfilzomib-sensitive PDPCCs have a higher UPR induction capacity than the resistant ones. Moreover, this differential sensitivity to carfilzomib treatment correlates positively with the nuclear levels of both ATF4 and CHOP and the genes associated with their pathways. Contrarily, ATF6 and chaperones, such as HSP90B1 and HSP5/GRP78, were highly expressed in the resistant PDPCCs. These results suggest that the PDAC-sensitive profile could be explained by the absence of an ER stress compensatory mechanism mediated by ATF6 and GRP78, and a lowest UPR threshold. The same pattern of sensitivity has been observed in multiple myeloma cells, and it was explained by the translational levels, where the PI-responsive tumors showed increased levels of protein synthesis (35). Following these observations, we measured the levels of transcription and protein synthesis in the PDPCCs before and after treatment. We detected that the sensitive cells have increased protein and RNA synthesis levels in comparison with the resistant PDPCCs, even after carfilzomib treatment. Also, we demonstrated that protein synthesis is critical in the carfilzomib sensitivity because translational inhibition protects the sensitive PDPCCs from cell death. The high levels of protein synthesis in a context of increased ATF4, which is related to translational suppression through eIF-2a phosphorylation, could be explained by the induction of PPP1R15A/GADD34, which promotes eIF-2a dephosphorylation and translational activation (55, 56). Finally, to further confirm the transcriptomic signature applicability to predict the carfilzomib chemosensitivity, BDPOs were used because it is a model that preserves some characteristics of the original tumor as differentiation and the ability to form 3 dimensional glands preserving the mucosecretory phenotype particularly in differentiated tumors. As expected, BDPOs showed a similar chemosensitivity compared with PDPCCs with a strong response in the sensitive BDPOs even at low carfilzomib concentration.

In summary, this is the first study to identify a transcriptomic stratification of PDAC based on the sensitivity to carfilzomib and to propose a putative molecular mechanism explaining the differential sensitivity. Furthermore, this finding contributes to the application of a personalized approach for the treatment of pancreatic cancer, associated with the capacity to identify the exceptional responsive patients independently of histologic or molecular classification, which could not characterize with enough accuracy the tumoral variability and consequently propose a therapeutic approach. Finally, here we confirm the possibility of using transcriptomic data to the repurposing of FDA-approved drugs for pancreatic cancer.

Disclosure of Potential Conflicts of Interest

No potential conflicts of interest were disclosed.

Authors' Contributions

N.A. Fraunhoffer: Resources, data curation, validation, investigation, methodology, writing-review and editing. **A.M. Abuelafia:** Resources, data curation, investigation. **M. Bigonnet:** Resources, validation. **O. Gayet:** Resources, validation, investigation. **J. Roques:** Resources, investigation. **E. Telle:** Resources, investigation. **P. Santofimia-Castaño:** Conceptualization, formal analysis, validation, investigation. **M.T. Borrello:** Investigation. **E. Chuluyan:** Conceptualization, supervision, investigation. **N. Dusetti:** Conceptualization, formal analysis, supervision, writing-original draft, writing-review and editing. **J. Iovanna:** Conceptualization, data curation, formal analysis, supervision, funding acquisition, writing-original draft, project administration, writing-review and editing.

Acknowledgments

This work was supported by INCa (grants number 2018-078 and 2018-079, BACAP BCB INCa_6294), Canceropole PACA, Amidex Foundation, Fondation de France, and INSERM. The authors wish to thank the CRCM Integrative Platform (Cibi), the CRCM's DataCentre for IT, and Scientific Computing (DISC).

The costs of publication of this article were defrayed in part by the payment of page charges. This article must therefore be hereby marked *advertisement* in accordance with 18 U.S.C. Section 1734 solely to indicate this fact.

Received April 2, 2020; revised May 27, 2020; accepted July 13, 2020; published first July 15, 2020.

References

1. McGuigan A, Kelly P, Turkington RC, Jones C, Coleman HG, McCain RS. Pancreatic cancer: a review of clinical diagnosis, epidemiology, treatment and outcomes. World J Gastroenterol 2018;24:4846–61.
2. Zhang Q, Zeng L, Chen Y, Lian G, Qian C, Chen S, et al. Pancreatic cancer epidemiology, detection, and management. Gastroenterol Res Pract 2016;2016: 8962321.
3. Campbell PJ, Yachida S, Mudie LJ, Stephens PJ, Pleasance ED, Stebbings LA, et al. The patterns and dynamics of genomic instability in metastatic pancreatic cancer. Nature 2010;467:1109–13.
4. Li D, Abbruzzese JL. New strategies in pancreatic cancer: Emerging epidemiologic and therapeutic concepts. Clin Cancer Res 2010;16:4313–8.
5. Hezel AF, Kimmelman AC, Stanger BZ, Bardeesy N, DePinho RA. Genetics and biology of pancreatic ductal adenocarcinoma. Genes Dev 2006;30:355–85.
6. Juiz NA, Iovanna J, Dusetti N. Pancreatic cancer heterogeneity can be explained beyond the genome. Front Oncol 2019;9:246.
7. Yachida S, Iacobuzio-Donahue CA. Evolution and dynamics of pancreatic cancer progression. Oncogene 2013;32:5253–60.
8. Bailey P, Chang DK, Nones K, Johns AL, Patch AM, Gingras MC, et al. Genomic analyses identify molecular subtypes of pancreatic cancer. Nature 2016;531:47–52.
9. Collisson EA, Sadanandam A, Olson P, Gibb WJ, Truitt M, Gu S, et al. Subtypes of pancreatic ductal adenocarcinoma and their differing responses to therapy. Nat Med 2011;17:500–3.
10. Lomberk G, Blum Y, Nicolle R, Nair A, Gaonkar KS, Marisa L, et al. Distinct epigenetic landscapes underlie the pathobiology of pancreatic cancer subtypes. Nat Commun 2018;9:1978.
11. Moffitt RA, Marayati R, Flate EL, Volmar KE, Loeza SGH, Hoadley KA, et al. Virtual microdissection identifies distinct tumor- and stroma-specific subtypes of pancreatic ductal adenocarcinoma. Nat Genet 2015;47:1168–78.
12. Chan-Seng-Yue M, Kim JC, Wilson GW, Ng K, Figueroa EF, O'Kane GM, et al. Author correction: transcription phenotypes of pancreatic cancer are driven by genomic events during tumor evolution. Nat Genet 2020;52:463.
13. Rashid NU, Peng XL, Jin C, Moffitt RA, Volmar KE, Belt BA, et al. Purity independent subtyping of tumors (PurIST), a clinically robust, single-sample classifier for tumor subtyping in pancreatic cancer. Clin Cancer Res 2020;26: 82–92.
14. Chan-Seng-Yue M, Kim JC, Wilson GW, Ng K, Figueroa EF, O'Kane GM, et al. Transcription phenotypes of pancreatic cancer are driven by genomic events during tumor evolution. Nat Genet 2020;52:231–40.
15. Nicolle R, Blum Y, Marisa L, Loncle C, Gayet O, Moutardier V, et al. Pancreatic adenocarcinoma therapeutic targets revealed by tumor-stroma cross-talk analyses in patient-derived xenografts. Cell Rep 2017;21:2458–70.
16. Bian B, Bigonnet M, Gayet O, Loncle C, Maignan A, Gilabert M, et al. Gene expression profiling of patient-derived pancreatic cancer xenografts predicts sensitivity to the BET bromodomain inhibitor JQ 1: implications for individualized medicine efforts. EMBO Mol Med 2017; 9:482–97.
17. Huang C, Lan W, Fraunhoffer N, Meilerman A, Iovanna J, Santofimia-Castaño P. Dissecting the anticancer mechanism of trifluoperazine on pancreatic ductal adenocarcinoma. Cancers 2019;11:1869.
18. Awasthi N, Schwarz MA, Schwarz RE. Combination effects of bortezomib with gemcitabine and EMAP II in experimental pancreatic cancer. Cancer Biol Ther 2010;10:99–107.
19. Boccadoro M, Morgan G, Cavenagh J. Preclinical evaluation of the proteasome inhbitor bortezomib in cancer therapy. Cancer Cell Int 2005;5:18.
20. Giaccone G. Clinical potential of proteasome inhibition in solid tumours. Eur J Cancer Suppl 2004;2:25–8.
21. Märten A, Zeiss N, Serba S, Mehrle S, Von Lilienfeld-Toal M, Schmidt J. Bortezomib is ineffective in an orthotopic mouse model of pancreatic adenocarcinoma. Mol Cancer Ther 2008;7:3624–31.
22. Shah SA, Potter MW, McDade TP, Ricciardi RA, Elliott PJ, Adams J, et al. 26S proteasome inhibition induces apoptosis and limits growth of human pancreatic cancer. J Cell Biochem 2001;82:110–22.
23. Potts BC, Albitar MX, Anderson KC, Baritaki S, Berkers C, Bonavida B, et al. Marizomib, a proteasome inhibitor for all seasons: preclinical profile and a framework for clinical trials. Curr Cancer Drug Targets 2011;11:25s4–84.
24. Mofers A, Pellegrini P, Linder S, D'Arcy P. Proteasome-associated deubiquitinases and cancer. Cancer Metastasis Rev 2017;36:635–53.
25. Smith GG. Proteasome inhibition in cancer therapy. J Infus Nurs 2005;28: 258–64.
26. Thibaudeau TA, Smith DM. A practical review of proteasome pharmacology. Pharmacol Rev 2019;71:170–97.
27. Voutsadakis IA. Proteasome expression and activity in cancer and cancer stem cells. Tumor Biol 2017;39:1010428317692248.
28. Moreau P, Richardson PG, Cavo M, Orlowski RZ, San Miguel JF, Palumbo A, et al. Proteasome inhibitors in multiple myeloma: 10 Years later. Blood 2012;120: 947–59.
29. Roeten MSF, Cloos J, Jansen G. Positioning of proteasome inhibitors in therapy of solid malignancies. Cancer Chemother Pharmacol 2018;81: 227–43.
30. Narayanan S, Cai CY, Assaraf YG, Guo HQ, Cui Q, Wei L, et al. Targeting the ubiquitin-proteasome pathway to overcome anti-cancer drug resistance. Drug Resist Updat 2020;48:100663.
31. Nencioni A, Hua F, Dillon CP, Yokoo R, Scheiermann C, Cardone MH, et al. Evidence for a protective role of Mcl-1 in proteasome inhibitor-induced apoptosis. Blood 2005;105:3255–62.
32. Gandolfi S, Laubach JP, Hideshima T, Chauhan D, Anderson KC, Richardson PG. The proteasome and proteasome inhibitors in multiple myeloma. Cancer Metastasis Rev 2017;36:561–84.
33. Manasanch EE, Orlowski RZ. Proteasome inhibitors in cancer therapy. Nat Rev Clin Oncol 2017;14:417–33.
34. Meister S, Schubert U, Neubert K, Herrmann K, Burger R, Gramatzki M, et al. Extensive immunoglobulin production sensitizes myeloma cells for proteasome inhibition. Cancer Res 2007;67:1783–92.
35. Obeng EA, Carlson LM, Gutman DM, Harrington WJ, Lee KP, Boise LH. Proteasome inhibitors induce a terminal unfolded protein response in multiple myeloma cells. Blood 2006;107:4907–16.
36. Duconseil P, Gilabert M, Gayet O, Loncle C, Moutardier V, Turrini O, et al. Transcriptomic analysis predicts survival and sensitivity to anticancer drugs of patients with a pancreatic adenocarcinoma. Am J Pathol 2015;185: 1022–32.
37. Kalari KR, Nair AA, Bhavsar JD, O'Brien DR, Davila JI, Bockol MA, et al. MAP-RSeq: Mayo analysis pipeline for RNA sequencing. BMC Bioinformatics 2014;15:224.
38. Anders S, Pyl PT, Huber W. HTSeq-A Python framework to work with high-throughput sequencing data. Bioinformatics 2015;31:166–9.
39. Biton A, Zinovyev A, Barillot E, Radvanyi FC. MineICA: independent component analysis of transcriptomic data. 2012.
40. Sergushichev AA. An algorithm for fast preranked gene set enrichment analysis using cumulative statistic calculation. bioRxiv 2016.
41. Liberzon A, Birger C, Thorvaldsdóttir H, Ghandi M, Mesirov JP, Tamayo P. The molecular signatures database hallmark gene set collection. Cell Syst 2015;1:417–25.
42. Schneider CA, Rasband WS, Eliceiri KW. NIH Image to ImageJ: 25 years of image analysis. Nat Methods 2012;9:671–5.
43. Venables WN, Ripley BD. Modern applied statistics with S. New York: Springer; 2002.
44. Ginestet C. ggplot2: elegant graphics for data analysis. J R Stat Soc Ser A Stat Soc 2011;174:245–6.
45. Gu Z, Eils R, Schlesner M. Complex heatmaps reveal patterns and correlations in multidimensional genomic data. Bioinformatics 2016;32: 2847–9.
46. Banno A, Garcia DA, Van Baarsel ED, Metz PJ, Fisch K, Widjaja CE, et al. Downregulation of 26S proteasome catalytic activity promotes epithelial-mesenchymal transition. Oncotarget 2016;7:21527–41.
47. Lee AH, Iwakoshi NN, Anderson KC, Glimcher LH. Proteasome inhibitors disrupt the unfolded protein response in myeloma cells. Proc Natl Acad Sci U S A 2003;100:9946–51.
48. Schröder M. Endoplasmic reticulum stress responses. Cell Mol Life Sci 2008;65: 862–94.
49. Urra H, Dufey E, Avril T, Chevet E, Hetz C. Endoplasmic reticulum stress and the hallmarks of cancer. Trends Cancer 2016;2:252–62.
50. Niewerth D, Jansen G, Assaraf YG, Zweegman S, Kaspers GJ, Cloos J. Molecular basis of resistance to proteasome inhibitors in hematological malignancies. Drug Resist Updat 2015;18:18–35.
51. Shah MH, Young D, Kindler HL, Webb I, Kleiber B, Wright J, et al. Phase II study of the proteasome inhibitor bortezomib (PS-341) in patients with metastatic neuroendocrine tumors. Clin Cancer Res 2004;10:6111–8.

Published OnlineFirst July 15, 2020; DOI: 10.1158/1078-0432.CCR-20-1232

52. Genovese G, Carugo A, Tepper J, Robinson FS, Li L, Svelto M, et al. Synthetic vulnerabilities of mesenchymal subpopulations in pancreatic cancer. Nature 2017;542:362–6.
53. Rolfe M. The holy grail: solid tumor efficacy by proteasome inhibition. Cell Chem Biol 2017;24:125–6.
54. Weyburne ES, Wilkins OM, Sha Z, Williams DA, Pletnev AA, de Bruin G, et al. Inhibition of the proteasome β2 site sensitizes triple-negative breast cancer cells to β5 inhibitors and suppresses Nrf1 activation. Cell Chem Biol 2017;24:218–30.
55. Iurlaro R, Munoz-Pinedo C. Cell death induced by endoplasmic reticulum stress. FEBS J 2016;283:2640–52.
56. Novoa I, Zeng H, Harding HP, Ron D. Feedback inhibition of the unfolded protein response by GADD34-mediated dephosphorylation of eIF2alpha. J Cell Biol 2001;153:1011–22.

Published OnlineFirst July 15, 2020; DOI: 10.1158/1078-0432.CCR-20-1232

Clinical Cancer Research

Evidencing a Pancreatic Ductal Adenocarcinoma Subpopulation Sensitive to the Proteasome Inhibitor Carfilzomib

Nicolas A. Fraunhoffer, Analía Meilerman Abuelafia, Martin Bigonnet, et al.

Clin Cancer Res 2020;26:5506-5519. Published OnlineFirst July 15, 2020.